Ultrasound Localization Microscopy Imaging by Monodisperse Microbubble Uncoupling: First Experimental Study

Giulia Tuccio[1], Lisa Te Winkel[2], Corinne Bruggeman[2], Wim Van Hoeve[2], and Libertario Demi[1]

[1]*Dept. of Information Engineering and Computer Science, University of Trento, Italy*
[2]*Solstice Pharmaceuticals, Enschede, the Netherlands*

***Abstract*—Ultrasound Localization Microscopy allows the characterization of micro-vascular structures by precisely localizing and tracking microbubbles (MBs) injected in the circulation. ULM-generated images possess a sub-millimetric resolution, overcoming the ultrasound's resolution limit set by diffraction. However, ULM requires low MBs concentrations to ensure isolated MBs signals. While low concentrations ensure MBs' localization precision, they lead to long acquisition times to fully cover the vascular structures in the region of interest. These prolonged acquisition times are not practical in the clinical setting. Here, towards the increase of MBs concentrations, we demonstrate the feasibility of uncoupling two monodisperse MB populations. The uncoupling is performed by means of a signal processing pipeline, which deploys the strong non-linear response of MBs having resonance frequency tuned with the transmission frequency. Density and flow direction maps are produced after data acquisition in a 3D-printed phantom and demonstrate the capability of uncoupling the two selected MB populations. The ability to discriminate different MBs populations mitigates ULM's low concentration requirement, allowing higher MBs concentrations, ultimately alleviating the need of long acquisition times for microvascular imaging.**

***Index Terms*—Ultrasound Contrast Agents, Monodisperse Microbubble, Ultrasound Localization Microscopy**

I. Introduction

ULTRASOUND Localization Microscopy (ULM) represents a milestone in ultrasound medical imaging context for micro-vascular characterization [1]. In fact, ULM overcomes the ultrasound's resolution limit set by diffraction, allowing to image microvascular structures with a sub-millimetric resolution. The information derivable from ULM-generated images could be used in the clinical context for a more thorough understanding of the circulatory system and its functioning. Furthermore, ULM could be helpful for the diagnosis and monitoring of diseases that alter the vasculature such as cancer, stroke, Alzheimer and Parkinson [1]–[3].

ULM generates images of the micro-vasculature by localizing and tracking injected MBs with a μm precision [1], [4], [5]. To ensure precise localizations, signals coming from each MB should be spatially isolated [6]. Failing to ensure sparsity of MBs signals, would cause MBs images to have overlapping signals. Because localization errors related to these situations are high, MBs with overlapping signals are usually excluded from the analysis. As a consequence, the acquisition times necessary to accumulate an adequate number of MBs events in the region of interest will substantially increase [1], [4]. However, the prolonged acquisition times are not practical in the clinical context owing to potential motion, increased computational load and patient comfort. Various groups have conducted research to shorten the acquisition times. To tackle the issue, methods include sparse recovery [7], [8], deconvolution [9] and velocity filtering [10]. Further, in [11], Huang et al. propose to define different sub-populations based on the different flow dynamics to separate overlapping MB signals. Nevertheless, all the aforementioned techniques rely on ultrafast plane wave imaging, which is out of reach for most clinical systems. In [12], the frame rates are reduced, but the MBs concentrations remain low, which constrains the technique to long acquisition times. Other approaches take advantage of the real-time response of deep learning architectures to localize MBs in dense scenarios [13], [14]. However, deep learning requires a significant amount of labeled data for model training and testing, which is not easily obtained.

In this study, we introduce the use of two monodisperse MB populations. Being able to uncouple these two, would allow to increase MBs concentrations, ultimately alleviating the need of prolonged acquisition times. Decreased acquisition times would be beneficial for ULM-generated maps quality while guaranteeing practical clinical procedures.

II. Materials and Methods

A. Monodisperse Microbubbles

To increase MB concentrations, we introduce a signal processing pipeline to uncouple two monodisperse MB populations. MB populations are selected to have a different frequency response, visible in Figure 2. In particular, we select:

1) P1: MB population generating mainly the fundamental harmonic response, having the resonance frequency not tuned with the transmission frequency;
2) P2: MB population generating a strong nonlinear response, having resonance frequency matching the transmission frequency.

The monodisperse populations are produced by Solstice Pharmaceuticals through a microfluidic chip, which allows control

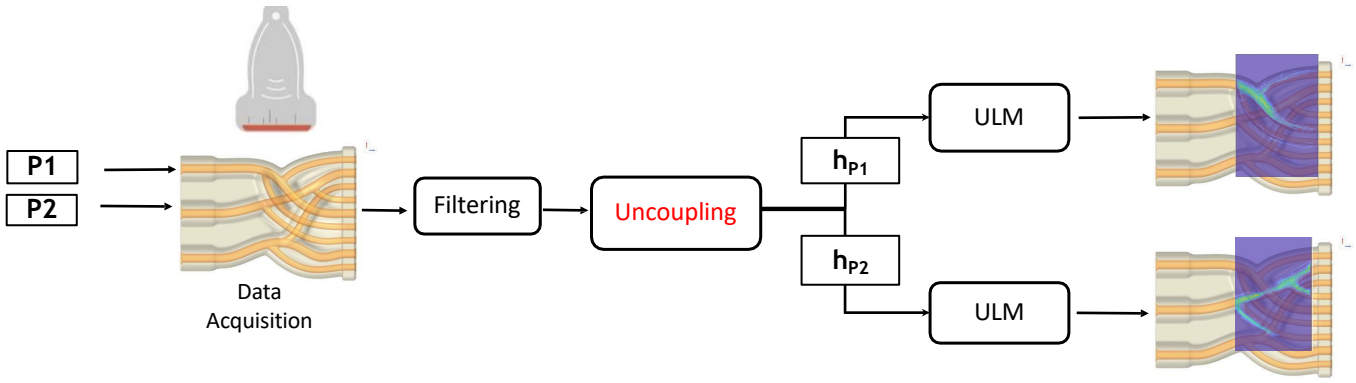

Fig. 1: Data acquisition and signal processing pipeline to uncouple the two MB populations (P1 and P2).

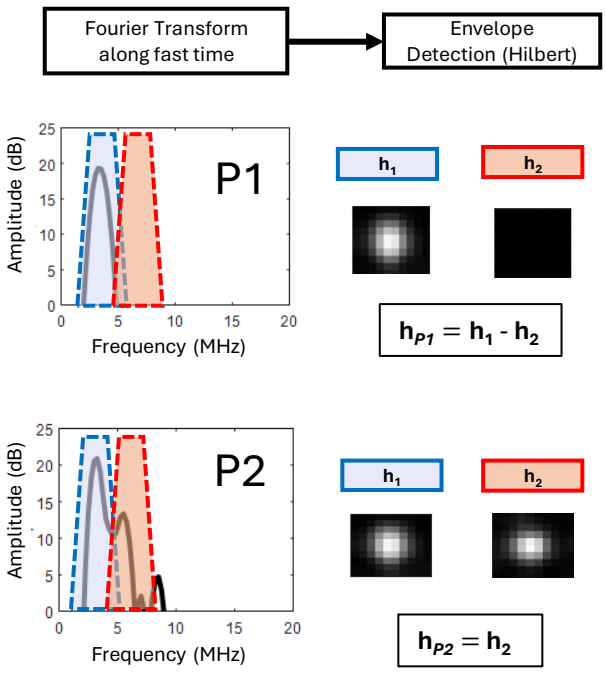

Fig. 2: Uncoupling of population P1 and P2. After performing the Fourier Transform along fast time for the first and second harmonic, the images of the first harmonic h_1 and second harmonic h_2 are generated by envelope detection. Finally, population P1 and P2 are obtained by $h_{P1} = h_1 - h_2$ and $h_{P2} = h_2$ respectively.

on the MBs diameter, thus on the resonance frequency [15], [16].

B. Proposed Approach

Ultrasound data are acquired when injecting each MB population in one channel of a 3D printed phantom, while flushing water in the other channel. The phantom's design (in Fig. 1), printing technology (Laser Syntering), and material (Flexa TPU) are selected in collaboration with PROM Facility, Rovereto, Italy. A programmable platform connected to a linear probe array (Esaote LA533) transmitting at 3 MHz and with 1 MHz of bandwidth is employed for imaging. After data acquisition, singular value decomposition is applied to filter the background static noise and the moving MBs signals ([17], [18]). Next, the uncoupling of the two MB populations is performed. The uncoupling produces two set of images, h_{P1} and h_{P2} for population P1 and P2 respectively. Particularly, P1 is imaged by subtracting the image of the first and the second harmonics ($h_{P1} = h_1 - h_2$), whereas P2 is displayed by imaging the second harmonic ($h_{P2} = h_2$), see Fig. 2. Finally, for each set of these images, density and flow direction maps are produced. ULM is implemented as a post-processing framework and includes MBs detection, localization and tracking (Figure 1). The detection is performed utilizing two methods. The first method is based on brightest pixels (method M1), whereas the second employs normalized cross-correlation between each ultrasound image and the MBs' PSF evaluated in water (method M2). For M2, only the MBs having a correlation above 0.5 are considered for localization. Localization is performed through Gaussian fitting ([19]) while tracking is performed through the Hungarian algorithm [1], [4], [19]. To improve tracking precision, MBs with persistence shorter than 7 frames are discarded. Finally, density and flow direction images are generated through accumulation.

III. Results

Figure 3 shows the reconstructed density and flow direction maps after uncoupling when imaging the population being injected (green background) and when imaging the population not being injected (red background). A perfect uncoupling would produce empty images in red background area. Figure 3 shows a better uncoupling capability of a model-based method (M2) with respect to a more naive method (M1). Results experimentally demonstrate the feasibility of monodisperse MBs

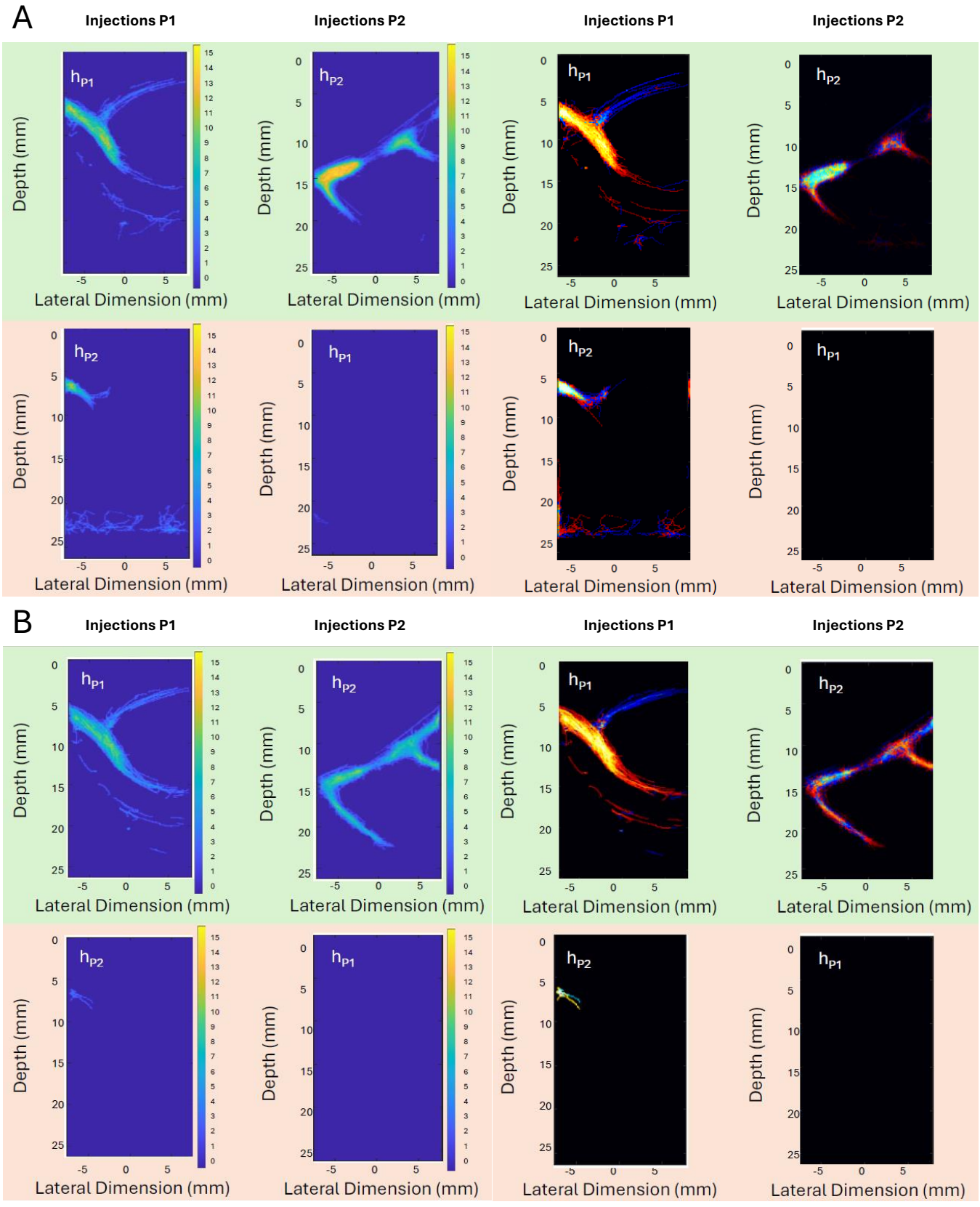

Fig. 3: ULM generated density (left) and flow direction (right) maps for population P1 (h_{P1}) and P2 (h_{P2}) for M1 (A) and M2 (B). The green background represents the images of P1 and P2 when injecting P1 and P2 respectively, whereas the red background highlights the images of P2 and P1 when injecting P1 and P2, respectively. For the flow direction maps, the color encodes flow direction. Red represents the flow away from the probe, whereas blue encodes flow towards the probe.

uncoupling, enabling the use of higher MBs concentrations for ULM, and thus potentially reducing acquisition time.

IV. Conclusion

In this study, we tested *in-vitro* the feasibility of uncoupling two monodisperse MB populations when injected singularly. ULM-generated density and velocity maps visually confirm the uncoupling capability of the proposed pipeline. As future work, we plan to test the uncoupling capability when injecting the two populations simultaneously. This would ultimately allow to increase MBs concentrations, thus alleviating the need of long acquisition time for micro-vascular imaging.

Acknowledgment

We thank PROM Facility, in Rovereto, Italy for the support in the 3D printing of the vascular phantom. In particular, M. Perini and C. Malacarne for 3D designing, material selection, and printing of the vascular phantom.

References

[1] O. Couture, B. Besson, G. Montaldo, M. Fink, and M. Tanter, "Microbubble ultrasound super-localization imaging (musli)," in *2011 IEEE International Ultrasonics Symposium*, 2011, pp. 1285–1287.

[2] A. Čarovac, F. Smajlovic, and D. Junuzovic, "Application of ultrasound in medicine," *Acta informatica medica : AIM : journal of the Society for Medical Informatics of Bosnia and Herzegovina : časopis Društva za medicinsku informatiku BiH*, vol. 19, pp. 168–71, 09 2011.

[3] N. Renaudin, C. Demené, A. Dizeux, N. Ialy-Radio, S. Pezet, and M. Tanter, "Functional ultrasound localization microscopy reveals brain-wide neurovascular activity on a microscopic scale," *Nature Methods*, vol. 19, pp. 1004 – 1012, 2022. [Online]. Available: https://hal.science/hal-03824902

[4] O. Couture, V. Hingot, B. Heiles, P. Muleki-Seya, and M. Tanter, "Ultrasound localization microscopy and super-resolution: A state of the art," *IEEE transactions on ultrasonics, ferroelectrics, and frequency control*, vol. 65, no. 8, pp. 1304–1320, 2018.

[5] C. Errico, J. Pierre, S. Pezet, Y. Desailly, Z. Lenkei, O. Couture, and M. Tanter, "Ultrafast ultrasound localization microscopy for deep super-resolution vascular imaging," *Nature*, vol. 527, no. 7579, p. 499—502, November 2015. [Online]. Available: https://doi.org/10.1038/nature16066

[6] K. Christensen-Jeffries, O. Couture, P. A. Dayton, Y. C. Eldar, K. Hynynen, F. Kiessling, M. O'Reilly, G. F. Pinton, G. Schmitz, M.-X. Tang, M. Tanter, and R. J. van Sloun, "Super-resolution ultrasound imaging," *Ultrasound in Medicine & Biology*, vol. 46, no. 4, pp. 865–891, 2020. [Online]. Available: https://www.sciencedirect.com/science/article/pii/S0301562919315959

[7] O. Solomon, R. J. G. van Sloun, H. Wijkstra, M. Mischi, and Y. C. Eldar, "Exploiting flow dynamics for super-resolution in contrast-enhanced ultrasound," 2018.

[8] A. D. Bar-Zion, O. Solomon, C. Tremblay-Darveau, D. R. Adam, and Y. C. Eldar, "Sushi: Sparsity-based ultrasound super-resolution hemodynamic imaging," *IEEE Transactions on Ultrasonics, Ferroelectrics, and Frequency Control*, vol. 65, pp. 2365–2380, 2017.

[9] J. Yu, L. Lavery, and K. Kim, "Super-resolution ultrasound imaging method for microvasculature in vivo with a high temporal accuracy," *Scientific Reports*, vol. 8, 09 2018.

[10] U. Soylu and Y. Bresler, "Circumventing the resolution-time tradeoff in ultrasound localization microscopy by velocity filtering," 2021.

[11] C. Huang, M. Lowerison, J. Trzasko, A. Manduca, Y. Bresler, S. Tang, P. Gong, U. W. Lok, P. Song, and S. Chen, "Short acquisition time super-resolution ultrasound microvessel imaging via microbubble separation," *Scientific Reports*, vol. 10, 04 2020.

[12] G. Tuccio, S. Afrakhteh, G. Iacca, and L. Demi, "Time efficient ultrasound localization microscopy based on a novel radial basis function 2d interpolation," *IEEE Transactions on Medical Imaging*, vol. 43, no. 5, pp. 1690–1701, 2024.

[13] R. J. G. van Sloun, O. Solomon, M. Bruce, Z. Z. Khaing, H. Wijkstra, Y. C. Eldar, and M. Mischi, "Super-resolution ultrasound localization microscopy through deep learning," *IEEE Transactions on Medical Imaging*, vol. 40, no. 3, pp. 829–839, 2021.

[14] Y. Shin, M. R. Lowerison, Y. Wang, X. Chen, Q. You, Z. Dong, M. A. Anastasio, and P. Song, "Context-aware deep learning enables high-efficacy localization of high concentration microbubbles for super-resolution ultrasound localization microscopy," *bioRxiv*, 2023. [Online]. Available: https://www.biorxiv.org/content/early/2023/04/23/2023.04.21.536599

[15] E. Castro-Hernández, W. Hoeve, D. Lohse, and J. Gordillo, "Microbubble generation in a co-flow device operated in a new regime," *Lab on a chip*, vol. 11, pp. 2023–9, 03 2011.

[16] W. van Hoeve, M. de Vargas Serrano, L. te Winkel, F. Forsberg, J. K. Dave, K. Sarkar, C. E. Wessner, and J. R. Eisenbrey, "Improved sensitivity of ultrasound-based subharmonic aided pressure estimation using monodisperse microbubbles," *Journal of Ultrasound in Medicine*, vol. 41, no. 7, pp. 1781–1789, 2022. [Online]. Available: https://onlinelibrary.wiley.com/doi/abs/10.1002/jum.15861

[17] K. Riemer, M. Lerendegui, M. Toulemonde, J. Zhu, C. Dunsby, P. Weinberg, and M.-X. Tang, "On the use of singular value decomposition as a clutter filter for ultrasound flow imaging," 04 2023.

[18] C. Demené, T. Deffieux, M. Pernot, B.-F. Osmanski, V. Biran, J.-L. Gennisson, L.-A. Sieu, A. Bergel, S. Franqui, J.-M. Correas *et al.*, "Spatiotemporal clutter filtering of ultrafast ultrasound data highly increases doppler and fultrasound sensitivity," *IEEE transactions on medical imaging*, vol. 34, no. 11, pp. 2271–2285, 2015.

[19] B. Heiles, A. Chavignon, V. Hingot, P. Lopez, E. Teston, and O. Couture, "Performance benchmarking of microbubble-localization algorithms for ultrasound localization microscopy," *Nature Biomedical Engineering*, vol. 6, 05 2022.